J. Fluid Mech. (1984), *vol.* 138, *pp.* 129–160
Printed in Great Britain

Numerical analysis of the flow through a corrugated tube with application to arterial prostheses

By C. N. SAVVIDES AND J. H. GERRARD
Department of the Mechanics of Fluids, University of Manchester

(Received 24 January 1983 and in revised form 19 September 1983)

Steady and oscillating axisymmetric laminar flows are determined by a finite-difference solution of the vorticity and continuity equations for an incompressible fluid contained in a straight concertina-shaped tube far from its ends. In steady flow the size of the wall corrugations is varied as well as the Reynolds number of the flow. In unsteady flow one tube geometry is studied, and the parameters varied are the Reynolds number, the ratio of the mean volume flow rate to its amplitude, and the frequency of oscillation. The analysis produces streamlines, particle paths and the pressure difference across a length of the tube. The resistance to the flow is determined in terms of an equivalent cylindrical tube diameter.

In steady flow the onset of flow separation and the growth of the separated region of flow is determined. The equivalent diameter is found to be principally a function of the product of Reynolds number and the non-dimensional pressure difference. This product depends on the height of the wall corrugations and less strongly on Reynolds number and the length of the corrugations. Resistance increases with increasing height of the corrugations. Comparison is made with other computational and experimental values of the pressure difference.

In unsteady flow the mean velocity to amplitude ratio has little effect except on the particle paths. The flow pattern is found to be governed by the Stokes number (radius $\times$ $(2\pi/(\text{kinematic viscosity} \times \text{period}))^{\frac{1}{2}}$) and the Reynolds number. There is a region of quasi-steady flow at the time of zero acceleration at maximum flow, but unsteady flow in between. The mixing produced by radial convection is restricted to the outer parts of the tube where the wall is corrugated. In oscillating flow the resistance relative to a cylindrical tube decreases as frequency and Reynolds number increase.

In the medical application of the work the concern is whether sustained stagnant regions occur in the corrugations and whether there is a large change in resistance relative to a cylindrical tube. This part of the investigation was made with an arterial waveform which contained six harmonics. It is found that there are no regions of stagnant fluid in the range of parameters considered. The difference between the variation with the flow parameters of the resistance of the corrugated tube and of a cylindrical tube was found not to be large.

1. Introduction

Interest in the subject of this paper has developed from a practical problem concerned with blood flow in arterial prostheses. The steady and oscillating flows in corrugated tubes are interesting from a purely fluid-mechanical point of view and

we present the work in this way. The medical applications will be discussed at the end in §7. This seems reasonable because the complicated nature of the medical problem involves as much biochemistry as fluid mechanics. The present work is a contribution to the practical problem, which will require further contributions from other disciplines before a final judgement can be made. The main purpose of this work is to examine the effect of the corrugations on the flow structure, that is, on flow separation and vortex formation. We will determine the effective skin friction by a derivation of the equivalent cylindrical tube which gives the same volume flow rate for the same pressure difference as the corrugated tube.

The determination of flow separation in steady flow is straightforward, but there is no precise definition of separation in unsteady flow. In the present work on oscillating flow some separation occurs during times in which the flow in the corrugation is slowly changing and hence quasi-steady. In these cases separation is clearly shown. When the flow is unsteady, as at times of approximately zero volume flow rate, separation would best be viewed in terms of particle paths because separation must mean that particles are moving from the wall region into the flow. Particle paths from all mesh points in the corrugation are followed in the work of §7, where it is seen that we may describe the flow as having separated in the corrugations.

The foundations of the analysis of the flow in the region of intersection between two walls has been laid by Moffatt (1964) and Smith (1976). We will consider our results on secondary separation at the apex of the corrugation in terms of Moffatt's theory. The work of Smith, though not directly comparable with the present work, shows that two-dimensional and axisymmetric flows have essentially the same characteristics and so comparison with the results of Sobey (1980) is reasonable.

The work and some of the results are similar to those of Sobey (1980), who treated the two-dimensional problem of large sinusoidal and semicircular corrugations bordering a narrow central channel. We consider an amplitude of corrugation which is relatively small compared with the overall diameter. There is some overlapping of the ranges of parameters studied and a comparison of results is possible.

There has been interest in the friction factor of steady laminar flow in corrugated tubes of various geometries as models of the flow through packed beds and porous rock. Reference will be made to the work of Batra, Fulford & Dullien (1970) and of Azzam & Dullien (1977). There are precise and well-documented experimental and numerical determinations of friction factor for steady flow in tubes with sinusoidal axial variation of radius by Deiber & Schowalter (1979). Specific comparison will be made with the results of this work. Computation of oscillating flow in a tube of varying radius has been made by Mirolyubov (1979). This work is similar to the present study but is not directly comparable.

A cross-section of the straight tube is shown in figure 1, where A and L are defined as the height and length of the corrugations of the wall of the tube of maximum diameter D. Also shown are the coordinates used later to refer to particle positions. We will refer to the intersection of the walls of the corrugation at the maximum radius as the apex of the corrugation and call the intersection at minimum radius the corner. Streamlines and particle paths are determined with a computational mesh numbered from 0 to 40 in the radial direction and from 0 to 16 in the axial direction across one corrugation ($M+N=40$, $N=8$ in figure 2). The problem is simplified for computational purposes by assuming that the flow is Newtonian, incompressible, laminar and axisymmetric. The walls are rigid and the flow in one corrugation is studied. It is

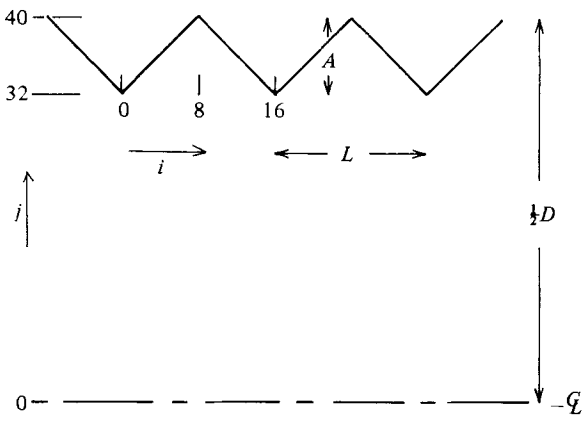

FIGURE 1. Corrugated-tube geometry and coordinates for particle positions in unsteady flow.

assumed that this is far from the tube entrance so that conditions at each end of the corrugation are identical. The fluid velocity is of the form

$$w = \overline{w} + \hat{w}\cos\frac{2\pi t}{T}, \tag{1}$$

where t is the time and T is the period of the oscillation. Quantities are non-dimensionalized with the maximum inside diameter D and with the cross-sectional-mean velocity amplitude $\hat{W}$ at that section. In steady flow where $\hat{W}$ is zero, $\overline{W}$, the mean velocity at the section of diameter D, is used as the characteristic velocity. The geometrical non-dimensional parameters are A/D and L/D. Dimensional analysis shows that the non-dimensional parameters of the flow are three of the following:

$$\text{the velocity ratio} \quad \epsilon = \overline{W}/\hat{W},$$

$$\text{the Reynolds number} \quad Re = WD/\nu,$$

$$\text{the Stokes number} \quad \alpha = 0.5D(2\pi/\nu T)^{\frac{1}{2}},$$

and

$$\text{the Strouhal number} \quad St = D/WT,$$

where ν is the kinematic viscosity coefficient of the fluid. The velocity W is $\overline{W}$ in steady flow, and in oscillating flow W is put equal to $\hat{W}$ even when the oscillation is about a non-zero mean. The overall characteristics of an oscillating flow will be found to depend on α and Re. St principally determines particle paths outside the corrugations. In steady flow the frequency parameters are absent and Re is the significant parameter. Capital letters are used to refer to cross-sectional-mean velocities and small letters to denote velocities which are functions of radial distance.

2. The numerical method

The computational procedure used to solve this problem is well known and has been widely used in recent years. The present computer program has been used for other work, on the point of submission for publication by G. Y. Buss, on oscillating flows in tubes of varying area and agreement obtained with analysis and experiments to within 1 or 2% for velocity magnitude. The discrepancy increases with Reynolds

number. The Navier–Stokes equations are transposed into the equations of vorticity and continuity, with vorticity and stream function as variables:

$$\frac{\partial \eta}{\partial t}+\frac{1}{r}\frac{\partial \psi}{\partial z}\frac{\partial \eta}{\partial r}-\frac{1}{r}\frac{\partial \psi}{\partial r}\frac{\partial \eta}{\partial z}-\frac{\eta}{r^2}\frac{\partial \psi}{\partial z}=\frac{1}{Re}\left[\frac{\partial^2 \eta}{\partial r^2}+\frac{1}{r}\frac{\partial \eta}{\partial r}+\frac{\partial^2 \eta}{\partial z^2}-\frac{\eta}{r^2}\right], \tag{2}$$

$$\eta=\frac{1}{r}\left[\frac{\partial^2 \psi}{\partial r^2}-\frac{1}{r}\frac{\partial \psi}{\partial r}+\frac{\partial^2 \psi}{\partial z^2}\right]. \tag{3}$$

The only non-zero component of vorticity is

$$\eta=\frac{\partial u}{\partial z}-\frac{\partial w}{\partial r}. \tag{4}$$

The Stokes stream function ψ is related to the r- and z-components of velocity u and w by

$$u=\frac{1}{r}\frac{\partial \psi}{\partial z}, \quad w=-\frac{1}{r}\frac{\partial \psi}{\partial r}. \tag{5}$$

A central finite-difference scheme is used with a two-time-level Dufort–Frankel substitution for the time-dependent terms as described by Roache (1972). The equations are the same as those used by Gerrard (1971) and Butler (1979), who dealt with axisymmetric-tube problems. Different facets of treatments similar to the present one are described by Pearson (1965), Macagno & Hung (1967), Williams (1969), Gillani & Swanson (1976) and Sobey (1980). The finite-difference forms of (2) and (3) give the updated values of the vorticity and stream function as

$$\begin{aligned}\eta_{i,j}^{k+1}&\left(1+\frac{\Delta t}{Re\,r^2}+\frac{2\Delta t(g^2+h^2)}{Re\,g^2h^2}\right)\Big/2\Delta t\\&=\eta_{i,j}^{k-1}\left(1-\frac{\Delta t}{Re\,r^2}-\frac{2\Delta t(g^2+h^2)}{Re\,g^2h^2}\right)\Big/2\Delta t+\left\{\frac{Re\,r}{4gh}[(\psi_{i+1,j}-\psi_{i-1,j})(\eta_{i,j-1}-\eta_{i,j+1})\right.\\&\quad+(\psi_{i,j+1}-\psi_{i,j-1})(\eta_{i+1,j}-\eta_{i-1,j})]+\frac{Re}{2g}\eta_{i,j}(\psi_{i+1,j}-\psi_{i-1,j})\\&\quad\left.+\frac{r^2}{h^2}(\eta_{i,j+1}+\eta_{i,j-1})+\frac{r}{2h}(\eta_{i,j+1}-\eta_{i,j-1})+\frac{r^2}{g^2}(\eta_{i+1,j}+\eta_{i-1,j})\right\}\Big/Re\,r^2,\end{aligned} \tag{6}$$

$$\begin{aligned}\psi_{i,j}^{k+1}=\Big\{&g^2(\psi_{i-1,j}+\psi_{i+1,j})+h^2(\psi_{i,j+1}+\psi_{i,j-1})\\&-\frac{gh^2}{2r}(\psi_{i,j+1}-\psi_{i,j-1})-g^2h^2r\eta_{i,j}^{k+1}\Big\}\Big/2(g^2+h^2).\end{aligned} \tag{7}$$

The non-dimensional mesh lengths in the r- and z-directions are g and h respectively. The subscripts i,j refer to mesh points in the z- and r-directions and the superscripts refer to the number of the time step. Where the superscript is omitted it is k. Thus the vorticity equation gives η_{ij} at time $(k+1)\,\Delta t$, where Δt is the time step, in terms of $\eta_{i,j}$ at time $(k-1)\,\Delta t$ and ψ and η values at adjacent mesh points at time $k\Delta t$. The solution of the finite-difference equations requires some initial and boundary conditions to be assigned and their computational stability must be ensured by using the right time step and mesh lengths.

2.1. *Initial and boundary conditions*

Initial values of η and ψ are needed at all mesh points. In some preliminary computations flows starting from rest were considered. This was found to produce

some numerical instabilities due to the large gradients occurring near boundaries and the computing time was very long. In all studies presented here a Poiseuille profile at each cross-section was initially assumed for η and ψ. This led to a more rapid convergence and reduced computing time considerably.

The boundary conditions imposed on (6) and (7) are

$$\psi = 0 \quad \text{on the tube axis;}$$

and on the boundary walls

$$\psi = \psi_B = \begin{cases} -0.125 & \text{for steady flow} \qquad (8) \\ -0.125\left(\epsilon + \cos\dfrac{2\pi t}{\mathrm{T}}\right) & \text{for oscillatory flow.} \qquad (9) \end{cases}$$

The boundary conditions at the entrance and exit of one wavelength of the corrugation are given by the periodic nature of the wall and the assumption that the tube is in effect infinitely long. Hence

$$\psi|_{z=0} = \psi|_{z=L}, \qquad (10)$$

$$\eta|_{z=0} = \eta|_{z=L}. \qquad (11)$$

Since the flow is axisymmetric $\eta = 0$ on the tube axis. Values of η on the boundary wall are determined by extrapolation from known values in the flow. This is done by expanding the stream function and vorticity at the wall in Taylor series and applying the conditions of no slip and zero normal velocity at the wall. Figure 2 shows the mean used for the computation and also the (p, m)-coordinate system used for the extrapolation. p is parallel and m normal to the wall. The wall makes an angle θ with the tube axis. The point on the sloping wall at which the value of η is required is B, and $B+1$ is the point where the normal to the wall at B crosses the next gridline. The distance from B to $B+1$ is $k = g/\cos\theta$. Applying a Taylor-series expansion at B for ψ and η gives

$$\psi_{B+1} = \psi_B - k\left(\frac{\partial\psi}{\partial m}\right)_B + \frac{k^2}{2}\left(\frac{\partial^2\psi}{\partial m^2}\right)_B - \frac{k^3}{6}\left(\frac{\partial^3\psi}{\partial m^3}\right)_B + \ldots, \qquad (12)$$

$$\eta_{B+1} = \eta_B - k\left(\frac{\partial\eta}{\partial m}\right)_B + \frac{k^2}{2}\left(\frac{\partial^2\psi}{\partial m^2}\right) - \ldots. \qquad (13)$$

The boundary conditions at B are

$$\left(\frac{\partial\psi}{\partial m}\right)_B = 0 \quad \text{(no-slip condition)},$$

$$\left(\frac{\partial\psi}{\partial p}\right)_B = 0 \quad \text{(no flow through the wall)},$$

$$\left(\frac{\partial^n\psi}{\partial p^n}\right)_B = 0 \quad (n = 1, 2, 3, \ldots),$$

(ψ constant along the wall).

The derivatives of ψ can be evaluated from the continuity equation (3), which after change of axes becomes

$$\eta = \frac{1}{r}\left[\frac{\partial^2\psi}{\partial m^2} + \frac{\partial^2\psi}{\partial p^2} - \frac{1}{r}\left(\cos\theta\frac{\partial\psi}{\partial m} + \sin\theta\frac{\partial\psi}{\partial p}\right)\right]. \qquad (14)$$

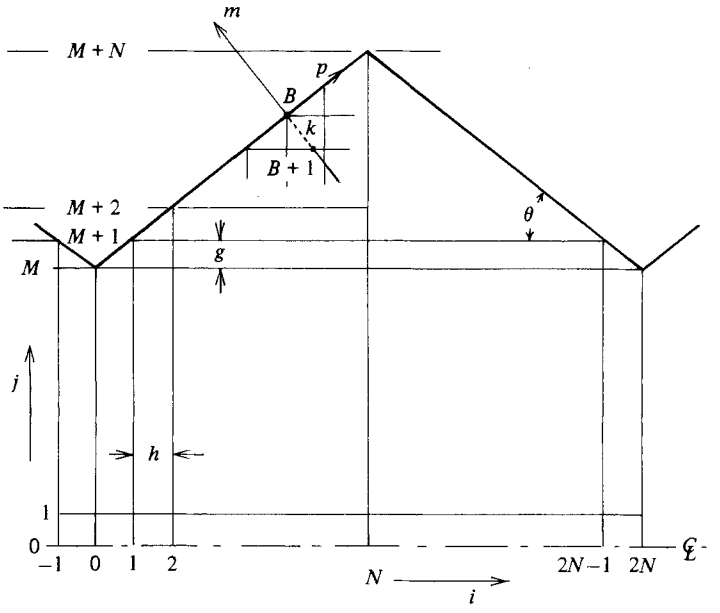

FIGURE 2. Grid system and coordinates for wall vorticity determination.

The application of the boundary conditions to this equation and its derivatives with respect to p and m gives expressions for the derivatives of ψ, and finally

$$\eta_B = \frac{\psi_B - \psi_{B+1} + \frac{k^2}{6}\eta_{B+1} r_B - \frac{k^3}{24}\left(\frac{2+\cos^2\theta}{\cos\theta}\right)\eta_{B+1}}{\frac{k^2}{3}\left[\frac{k}{2}\left(\frac{1+\cos^2\theta}{\cos\theta}\right) - r_B\right] - \frac{k^3}{24}\left(\frac{2+\cos^2\theta}{\cos\theta}\right)}. \tag{15}$$

At the corners of the corrugations θ is assumed to be zero. In this zero-inclination condition (15) reduces to the equation derived by Gerrard (1971) for a cylindrical tube. The values at $B+1$ are obtained by linear interpolation.

2.2. *The mesh size and time step*

The finite-difference form of the equations must satisfy certain requirements in order to reproduce faithfully a true solution of the continuous equations. The choice of time step and mesh length is governed by considerations of accuracy, computational stability and compatibility with the boundary data. The last requirement implies that Δt must be small compared with the timescale over which the boundary values are changing. This means that the mesh length Δx divided by the time step Δt must be greater than the rate at which vorticity diffuses away from its origin at the wall.

The relations involving mesh lengths and time step depend on the particular problem and must be found by trial and error. In the steady-flow case two expressions for Δt were available:

$$\Delta t > \frac{1}{15}\frac{h^2 g^2 Re}{h^2 + g^2} \tag{16}$$

and

$$\Delta t < \tfrac{1}{30} h^2 Re. \tag{17}$$

The expression giving the smaller value of Δt was used. In the oscillating-flow case

$$\Delta t < \frac{\alpha^2 h^2 T}{15\pi} \tag{18}$$

was used, where α is the Stokes number and T the period of the oscillation. Similar limits, obtained from program-stability considerations, were used by Williams (1969), who obtained $\Delta t < \frac{1}{8}h^2 Re$, and by Thoman & Szewczyk (1964).

The non-dimensional mesh lengths varied between 0.01 and 0.032 depending on L/D and A/D, and were computed from

$$h = \frac{L}{2ND}, \quad g = \frac{A}{ND} = \frac{1}{2(M+N)}, \tag{19}$$

where M and N are the number of grid points. There are $2N$ grid points in the axial direction and $M+I$ grid points in the radial direction, with $I = 0, 1, 2, \ldots, N$ as shown in figure 2. Mesh size was varied to obtain an indication of the accuracy in steady flow. Changing (M, N) from (20, 5) to (32, 8) to (48, 12) produced maximum changes in ψ of 0.2 % and 0.16 % of the wall value of ψ. The non-dimensional pressure drop over the corrugation (p^* of §4) changed by 2 % and 0.5 %. Particle paths were determined by a first-order difference scheme, but with Δt as small as indicated by (16)–(18) this is not expected to produce a noticeable error.

When the radial meshlines pass through the apexes of the corrugation the latter are points of discontinuous changes of slope. In some programs the apexes were made to fall midway between two radial meshlines. In this case the corners were rounded. Both types of mesh disposition have been used and only slight differences observed in particular in the determination of the Reynolds number for the onset of separation. This will be referred to later in connection with figure 9.

3. Computation of the steady flow

For steady flow the geometrical parameters and the Reynolds number are varied over ranges which demonstrate the variation of the separated region of flow and which include the range of practical interest for by-pass graft prostheses. One of each of the three parameters L/D, A/D and Re is varied at a time.

The variation with changing L/D is shown in figures 3 and 4. In these diagrams of computed streamlines and following similar figures for steady flow, lines of specific constant values of the stream function are drawn as indicated in the caption of figure 3. The flow is from left to right. In those figures in which there are closed streamlines the flow rotation is counterclockwise. The lines along which the stream function has the boundary value of -0.125 are indicated by + symbols. These are the separation–reattachment streamlines. These + symbols are separated by one mesh length in the axial direction. The separation and reattachment positions cannot be determined to better than half of a mesh length and so are not indicated. At a large-enough value of L/D the flow does not separate and the streamlines follow the wall shape. As L/D decreases below some critical value the flow separates at the apex of the corrugation as in figure 7 at $A/D = 0.1$. We shall refer to the point of maximum internal diameter of the tube as the apex of the corrugation and call the point of minimum internal diameter the corner. After its inception at the apex the separation region then grows as L/D decreases, eventually filling most of the corrugation. This is to be expected since the adverse pressure gradient is larger when the angle of inclination of the wall is larger. As will be seen the separation is more pronounced at higher Reynolds number. The critical L/D for the flow to separate increases as Re and A/D increase. This can be seen from figure 4, where $2S/LA$ is shown as a function of L/D for various Re; $2S/LA$ is the ratio of the area S of the cross-section of the separated region to the triangular area of cross-section of the corrugation. It is seen that for $Re = 100$

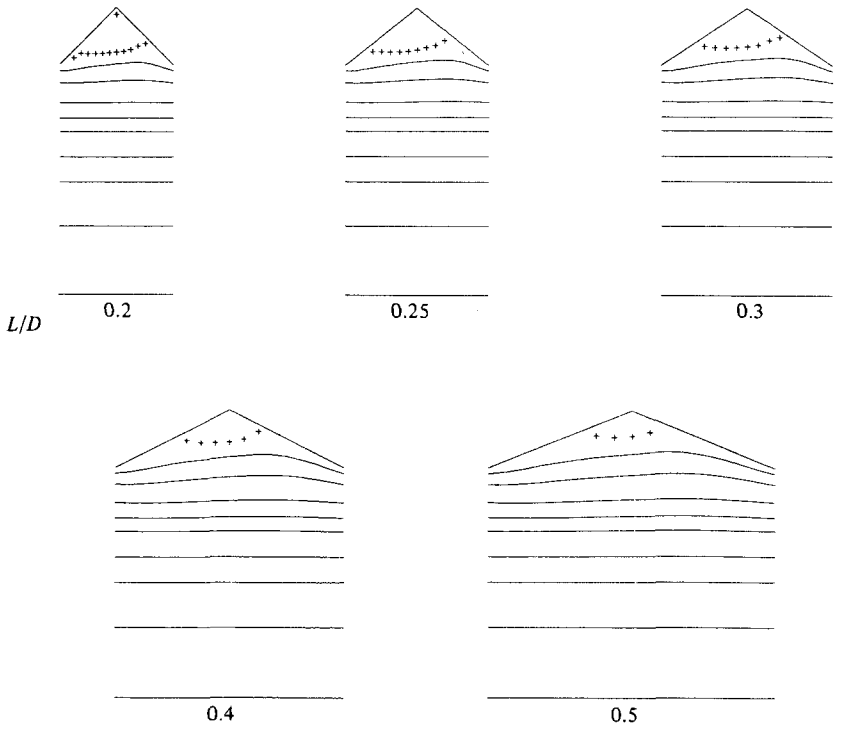

FIGURE 3. Streamlines of steady flow at $Re = 250$, $A/D = 0.1$. Values of $-\psi$ in steady-flow streamline figures are 0, 0.02, 0.05, 0.07, 0.09, 0.10, 0.11, 0.12, 0.124, 0.125.

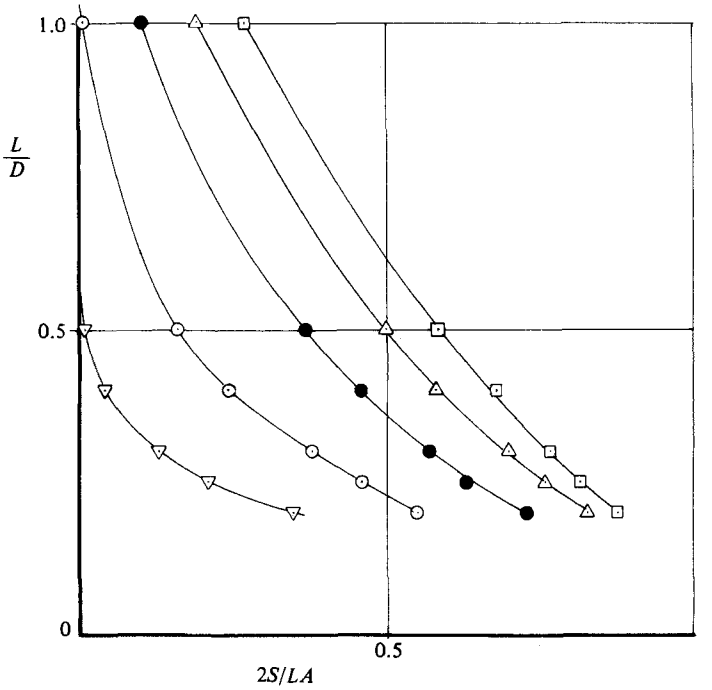

FIGURE 4. Ratio of separated area to corrugation area as a function of L/D for various Reynolds numbers and $A/D = 0.1$: ▽, $Re = 100$; ○, 250; ●, 500; △, 750; □, 1000.

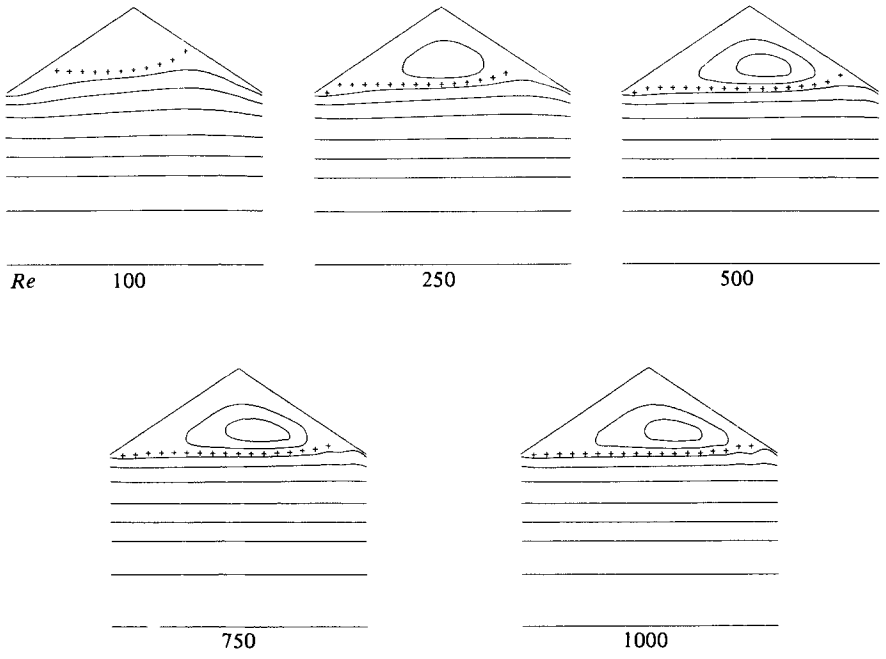

FIGURE 5. Streamlines of steady flow at $L/D = 0.5$, $A/D = 0.167$. Values of $-\psi$ extra to figure 3 are 0.126 and 0.127.

and $A/D = 0.1$ the lowest L/D for which separation does not occur is about 0.55, and for $Re = 250$ and $A/D = 0.1$ it is about 1.06.

The effect of the Reynolds number on the flow is considered next for a particular A/D and L/D. Figure 5 shows the streamlines for $L/D = 0.5$ and $A/D = 0.167$ as the Reynolds number increases from 100 to 1000. Separation first occurs at a small Reynolds number, as we see from figure 6. The separated region grows with increasing Reynolds number, and the vortex formed spreads, shifting its centre downstream. This shift is more pronounced at larger values of A/D. Curves showing the variation of separation area with Re at constant L/D and A/D are plotted in figure 6. Extrapolation of these curves will give the maximum Re, Re_0, for which there is no separation. For this reason exponential curves of the form

$$S' = S'_\infty(1-\exp(-k(Re-Re_0)))$$

are drawn to pass through the points as well as possible. S' is written for $2S/LA$, S'_∞ is the fractional separated area at infinite Reynolds number. It is seen that the curves fit the points reasonably well. The extrapolations indicate that for two of the six cases separation occurs at zero Reynolds number. These two geometries have walls making the largest angles to the axis. This is in agreement with the analysis of Moffatt (1964). The interpretation of Moffatt's work in this context is that when there is a significantly sized region at the apex in which the local Reynolds number is small an eddy will be seen. This will occur at low Reynolds number and large inclination of the wall to the tube axis. Moffatt's analysis also explains the absence of eddies and thus of separation at the corner of the corrugation.

Figure 7 shows the effect of varying A/D at constant values of Re and L/D. Extra streamlines are included to show the circulation within the separated region. If, following Sobey (1980), we relate the strength of the vortex to the difference between the wall value of the stream function and the minimum stream-function value in the

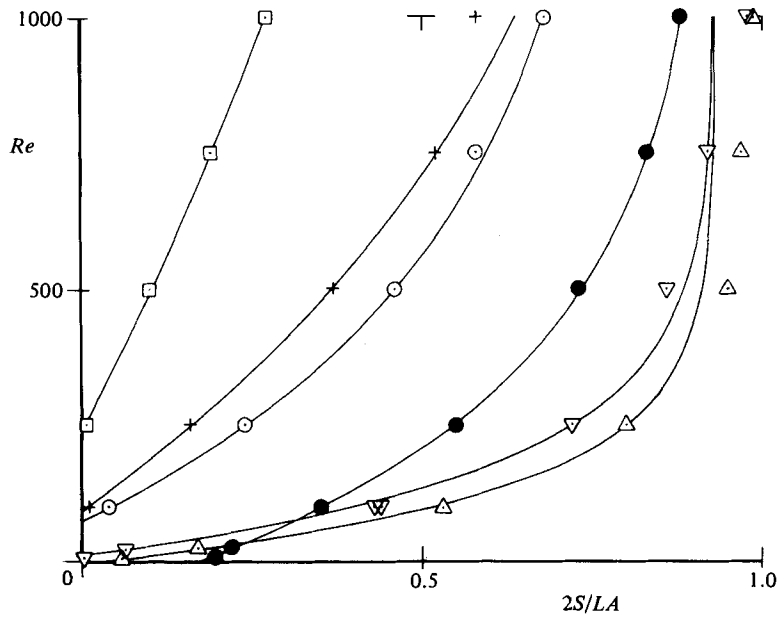

FIGURE 6. Ratio of separated area to corrugation area as a function of Reynolds number; computed points and exponential curves.

Symbol	L/D	A/D
□	1.0	0.1
+	0.5	0.1
○	0.4	0.1
●	0.2	0.1
▽	0.5	0.167
△	0.4	0.167

flow, we see that the vortex strength increases as A/D increases. We have plotted our minimum stream-function values against Re for various A/D and seen that the curves are of the same shape as Sobey's except that they become flatter at high Re. The minimum stream function corresponds to the reverse flow in the separation region, which is not simply relatable to the vortex strength or circulation. Figure 8 shows an alternative, but still inexact, representation of vortex strength. The circulation of the separated region is the line integral of the velocity along the separation streamline. As S grows larger the separated streamline moves into regions of higher speed as well as getting longer. $2S/LA$ is related to the length of this bounding line. Figure 8 clearly shows that the vortex strength increases rapidly with A/D at all Re, and also increases with Re at fixed A/D up to Re approaching 1000, where the variation is much diminished.

We have determined for the flows in figure 6 the smallest Re for which separation occurs. A plot of the vorticity at the apex of the corrugation as a function of the parameters gives the same information. Wall vorticity at the apex, where separation first occurs, changes sign when separation takes place. Several examples of these curves are shown in figure 9, from which secondary and also tertiary separation can be seen to take place. The abscissa chosen for figure 9 is the included angle at the apex. We see that as this angle decreases the curves for different parameter values become (approximately) dependent only on this angle. This is as we would expect from the theory of Moffatt (1964). The local Reynolds numbers in this region are small. The secondary and tertiary separations occur within one radial mesh length of the

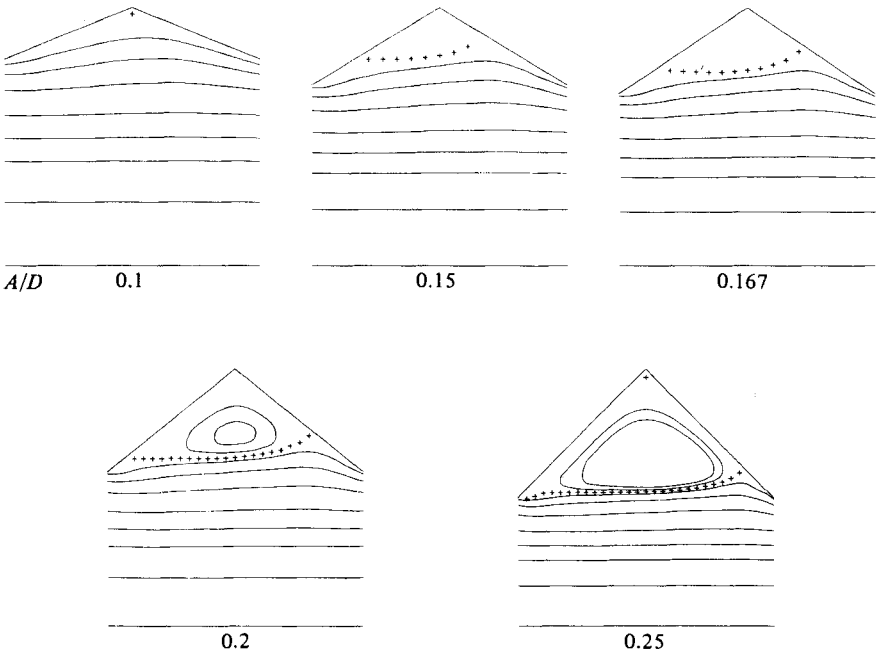

FIGURE 7. Streamlines of steady flow at $L/D = 0.5$, $Re = 100$. Values of $-\psi$ as in figure 5.

apex and the Reynolds numbers based on this mesh length and the local velocity for all the curves of figure 9 lie between 7×10^{-3} and 9×10^{-2}, and so we would expect Moffatt's theory to apply. All the other results presented here were found to be functions of L and A separately and not of A/L. The three points plotted as $S = 0$ on figure 8 were obtained from figure 9. The onset of separation at the apex is sensitive to the disposition of the computational mesh as described in §2.2. The differences produced are not large and are in the direction to be expected from the fact that when the apex lies between two mesh points it is effectively more rounded than when the apex is a mesh point.

The main characteristics of the flows computed are the same as those found by Sobey, as one would have expected. The geometry studied by Sobey was two-dimensional and his corrugations were sinusoidal and semicircular regions bordering a relatively narrow central channel, thus being comparable to larger values of A/D than considered here. The vortex produced by the separation shifts downstream as Reynolds number increases and secondary vortices are formed in deep corrugations. The vortex grows to fill the corrugation at higher Reynolds numbers, and here we have found that this also occurs as A/D increases at constant Reynolds number. In the present work the way in which the separated region depends on the parameters of the problem has been treated in greater detail. The wall vorticity at the corrugation apex shows the same type of variation in the two-dimensional and in the present work, though the numerical values are not the same. It is noteworthy that separation commences at the apex whether this is sharp or rounded.

4. The equivalent cylindrical tube in steady flow

The aim of the work is to predict blood flow in arterial bypass grafts, and thus the results obtained for steady flow with separation are irrelevant to the application. It does, however, serve as an introduction to the oscillating-flow case to consider the

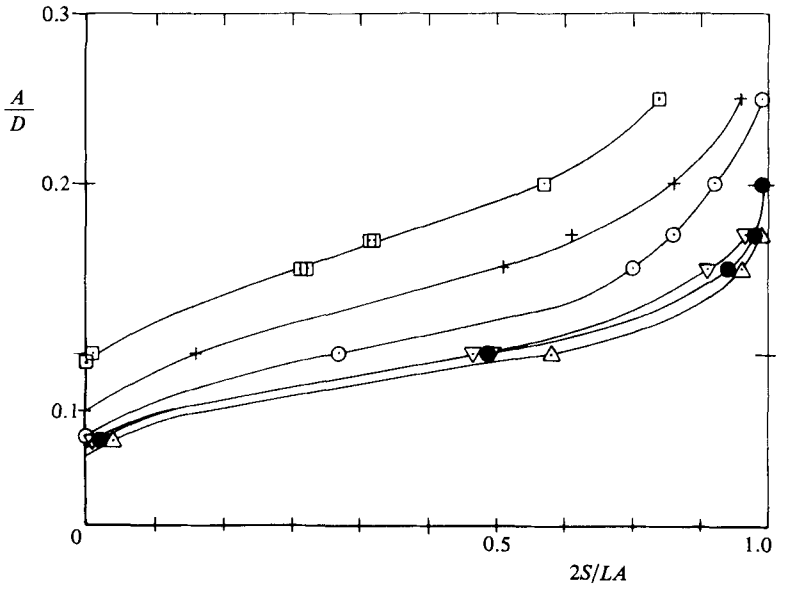

FIGURE 8. Ratio of separated area to corrugation area as a function of A/D.

Symbol	L/D	Re
□	0.5	100
+	0.5	250
○	0.5	500
▽	0.4	750
●	0.5	1000
△	0.4	1000

pressure difference across a corrugation and to determine the equivalent cylindrical tube. The cylindrical tube is equivalent when the pressure difference across it and the volume flow rate through it are both the same as in the corrugated tube. We define the non-dimensional pressure difference as

$$p^* = \frac{\Delta p}{L}\frac{D}{\rho \overline{W}^2}, \tag{20}$$

where Δp is the pressure difference between the ends of the corrugation and is computed by rearranging and integrating the axial equation of motion. The equation to be evaluated is

$$\int_{r_j, z_1}^{r_j, z_2} \frac{\partial}{\partial z}(p+\tfrac{1}{2}v^2)\,\mathrm{d}z = \int_{r_j, z_1}^{r_j, z_2}\left(u\eta - \frac{1}{Re}\frac{\partial \eta}{\partial r} - \frac{\eta}{r\,Re} - \frac{\partial w}{\partial t}\right)\mathrm{d}z, \tag{21}$$

where $v^2 = u^2 + w^2$. To verify that this can be derived from the equation of motion, we differentiate (21) with respect to z, put $\eta = \partial u/\partial z - \partial w/\partial r$ and use the continuity equation

$$\frac{\partial u}{\partial r} + \frac{\partial w}{\partial r} + \frac{u}{r} = 0$$

differentiated with respect to z. This gives

$$\frac{\partial w}{\partial r} + u\frac{\partial w}{\partial r} + w\frac{\partial w}{\partial z} = -\frac{\partial p}{\partial z} + \left[\frac{\partial^2 w}{\partial r^2} + \frac{1}{r}\frac{\partial w}{\partial r} + \frac{\partial^2 w}{\partial z^2}\right]\Big/ Re.$$

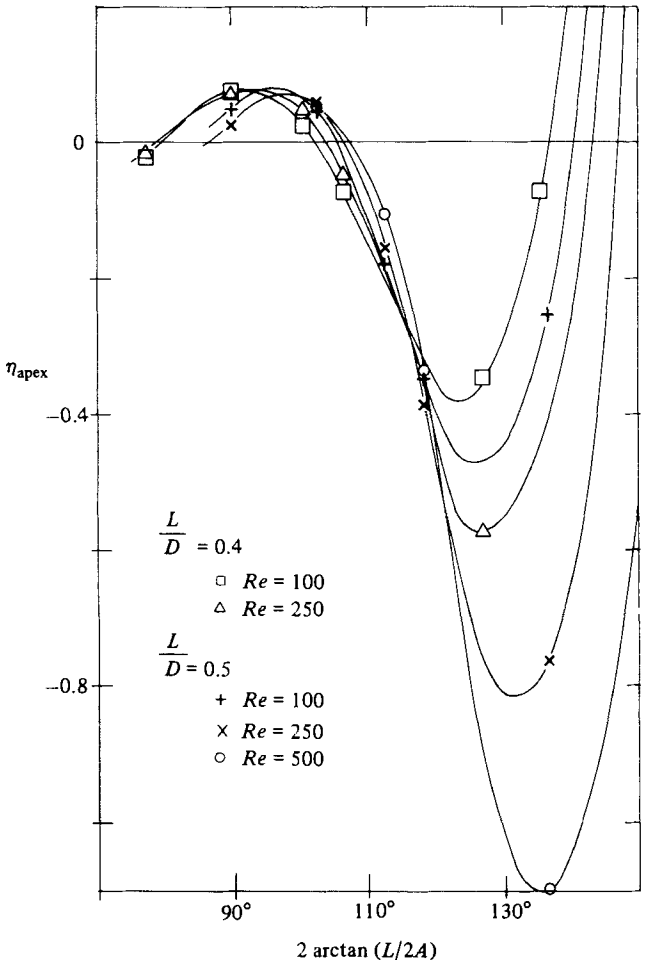

FIGURE 9. Vorticity at the apex of the corrugation as a function of the angle at the apex: $L/D = 0.4$: ⊡, $Re = 100$; △, 250. $L/D = 0.5$: +, $Re = 100$; ×, 250; ⊙, 500.

The left-hand side of (21) is Δp_{rj}, since v is the same at the entrance and exit. Integration over the cross section gives

$$\Delta p = \frac{2}{R^2}\int_0^R \left(u\eta - \frac{1}{Re}\frac{\partial \eta}{\partial r} - \frac{\eta}{Re\, r} - \frac{\partial w}{\partial t}\right) r\, \mathrm{d}r,$$

which is evaluated numerically.

The non-dimensional pressure difference p^* is proportional to the friction factor which is widely used in describing the pressure drop in pipe flow. There are three contributions to p^*: the corrugated tube has a bigger surface area than the equivalent cylindrical tube; the velocity gradient at the wall is different from that in cylindrical tube flow; the inclination of the wall implies that there is a component of the normal pressure force in the axial direction. For laminar flow in a cylindrical tube $Re\, p^*$ is constant because the volume flow rate Q is proportional to $D^4 \Delta p/L$. In a corrugated tube at Re-values small enough for inertia effects to be small, $Re\, p^*$ is still independent of Re but is increased above the cylindrical tube value of 32. This may be viewed as replacing D by D_e, the equivalent cylindrical tube diameter, and since D_e is less than D it follows that $Re\, p^*$ is increased. The increase is due to higher velocity

gradients at the walls, which have a larger surface area. There is also an asymmetry between the flows in the expanding and contracting parts of the corrugation. This asymmetry is visible just after separation in figure 7. Once separation has taken place the size of the separation region is a function of Re, and Rep^* becomes a function of Reynolds number – but this we shall see is not a strong effect, presumably because the three contributions to p^* do not all act in the same direction. It transpires that for our range of the parameters the pressure gradient is only weakly dependent on L/D and depends principally on Re and A/D; graphs of $Re\,\Delta p$ against L/D lie very close to straight lines passing through the origin with slopes depending on A/D.

In order to determine the diameter of the equivalent cylindrical tube we write (20) as

$$p^* = \frac{\Delta p}{LQ^2}\frac{\pi^2 D^5}{16\rho} = kD^5, \tag{22}$$

where k is a constant from the definition of the equivalent cylindrical tube. In the equivalent cylindrical tube k must have the same value, and so

$$k = p_e^*/D_e^5,$$

where suffix e denotes the value for the equivalent cylindrical tube for which $p_e^* = 32/Re_e$. Also $Re_e = D\,Re/D_e$, because $Re \propto 1/D$ at constant Q. We thus arrive at

$$\frac{D_e}{D} = \left\{\frac{32}{Rep^*}\right\}^{\frac{1}{4}}. \tag{23}$$

In figure 10 we plot Rep^* as a function of A/D for various Re and L/D values. The curve drawn has the equation

$$\frac{D_e}{D} = \frac{d}{D} + 0.05, \tag{24}$$

where $d = D - 2A$ is the minimum diameter of the corrugated tube. This curve is a fair representation of the computed results, except at small values of A/D, where it does not pass through the cylindrical-tube value of 32 at $A/D = 0$. From figure 10 we see that for each value of A/D the tube resistance and Rep^* increase as Re increases. Resistance increases as L/D decreases, as one would expect with a rougher wall, but in our range of values the resistance variation is slight. Large values of L/D will be referred to shortly. From figure 10 and (22) one can determine the pressure gradient and equivalent cylindrical-tube diameter corresponding to any particular geometry and Reynolds number within the range covered here. For small corrugations the resistance of the tube in steady flow is such that it is equivalent to a cylindrical tube of diameter equal to the maximum diameter of the corrugated tube. As A/D increases, the diameter of the equivalent cylindrical tube approaches the inside diameter of the corrugated tube. For a fixed maximum diameter D of the corrugations the resistance increases as A/D increases. Though the range of equivalent diameter is not very great, the fourth-power relationship in (23) results in the 10-fold increase in resistance shown in figure 10.

There are several published papers on the computation of steady flow in periodically constricted tubes. Most of this work concerns the friction factor as a function of Reynolds number. There is to our knowledge only one paper giving experimental results with sufficient documentation and accurate definition of wall shape with which we can compare our computations, and this is the work of Deiber & Schowalter (1979). They have made measurements and have computed the friction factor of a tube of mean radius a and with sinusoidal radius variation of amplitude ϵ. Our p^* and their

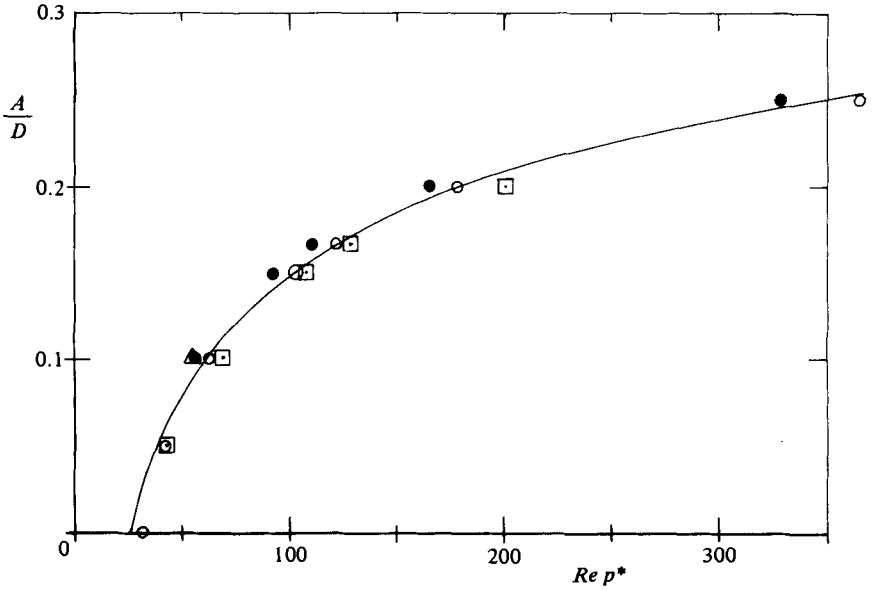

FIGURE 10. Variation of the product of Reynolds number and non-dimensional pressure gradient with A/D. The curve plotted is (24).

Symbol	Re	L/D
●	100	0.5
○	250	0.4
△	250	1.0
□	1000	0.4

friction factor f are related by $Re\,p^* = 2fN(1+\epsilon/a)^4$, where N is Deiber & Schowalter's Reynolds number; $Re = N/(1+\epsilon/a)$. We compare results for the same values of the wavelength of the sinusoidal corrugation, which we equate to L, and we equate twice the amplitude 2ϵ with our length A. All the computations and experiments of Deiber & Schowalter are for much larger L/D values than the ones that are relevant to the present application, and so for the comparison we have made a check at $L/D = 2.41$ and $A/D = 0.231$ corresponding to their figure 5. This figure is a log–log plot of friction factor versus Re, on which in viscous-dominated flow at low Reynolds number the results of computation and experiment lie on a straight line of slope -1 corresponding to $Re\,p^* =$ constant as in Poiseuille flow. Figure 11 is the same figure reproduced in our equivalent notation. The straight line of Deiber & Schowalter corresponds to $Re\,p^* = 145$. The accuracy of this value is about $\pm 3\,\%$ owing to reading values from their graph. Their computations and experiments depart from this line at $Re \approx 60$, which they say is where separation begins. It is surprising that curvature is not apparent at lower Reynolds numbers, because the streamlines show asymmetry before separation in the way of the pattern at $A/D = 0.1$ in figure 7. The effect of this asymmetry must be small.

Our computations of p^* were made at $Re = 10$, 50, 100 and 200, and the resulting values of $Re\,p^*$ were 142.5, 151.0, 167.8 and 188 respectively. Our point at $Re = 10$ lies on the Deiber & Schowalter curve. Our other points lie on a straight line on the log–log plot to within 0.7 %, and this line intersects the $Re\,p^* = 145$ line at $Re = 40$, which is about where separation begins (separation has just begun at the apex at $Re = 50$). These points at $Re = 50$–200 coincide with the experimental values of Deiber & Schowalter and lie twice as far from the $Re\,p^* = 145$ line as do their computed results.

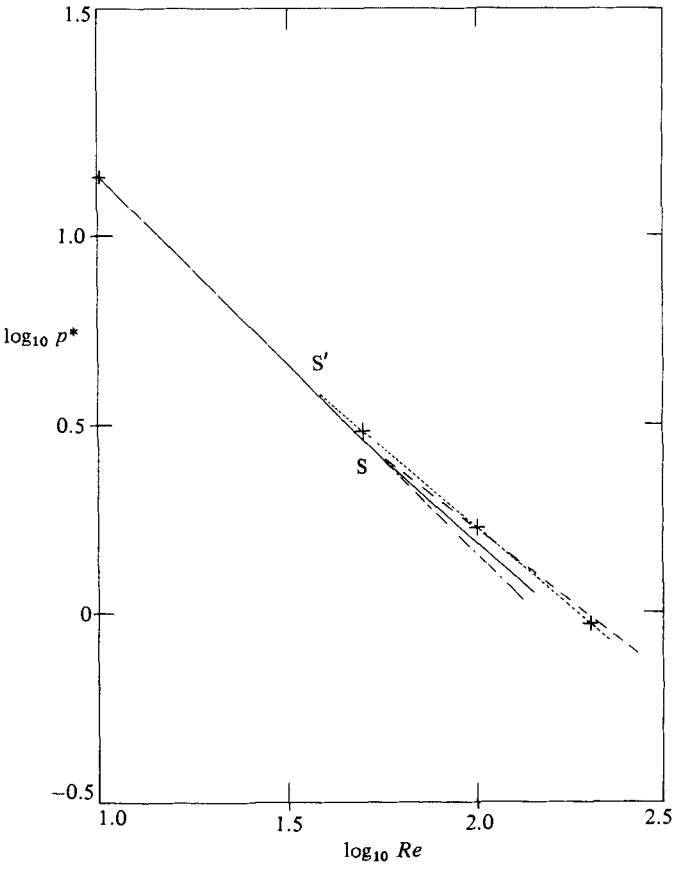

FIGURE 11. Graph equivalent to figure 5 of Deiber & Schowalter (1979). ——, Deiber & Schowalter computation; – – –, Deiber & Schowalter experiment (wall-radius variation sinusoidal); ---+----, present computation; S, Deiber & Schowalter, separation inception; S', present results, separation inception.

These observations do not serve as a check of accuracy of computation because of the difference in geometry. As was stated in §2, our results have been independently checked with analysis and experiment. The agreement with Deiber & Schowalter at low Reynolds number means that the increased resistance due to the sharp corner and apex of our triangular wall profile is balanced by the increased resistance due to a larger wall inclination midway between the corner and apex in the case of the sinusoidal wall profile. The larger departure of our results from the $Re\,p^* = 145$ line at higher Reynolds numbers is presumably also due to the effects of the difference in geometry; that our computations agree with the Deiber & Schowalter experiments is no doubt fortuitous. In our case the departure from the straight line of slope -1 ($Re\,p^*$ = constant) amounts at $Re = 200$ to 26 % of p^*. At smaller values of A/D and L/D the effect of Reynolds number in producing curvature in the relationship between p^* and Re is much less, as is also seen in the computations of Batra *et al.* (1970) and of Azzam & Dullien (1977).

Some computations have been made at Reynolds numbers less than 100 at $A/D = 0.167$ and smaller values. The results do not show the large increase in $Re\,p^*$ with Re which Deiber & Schowalter find from computation at $A/D = 0.375$ in their figure 2. This is presumably an effect of the narrowness of the central core of the flow when the constriction is so severe.

5. Computation of the oscillating flow

We turn now to the more practical but more complicated unsteady flow in a corrugated tube. The oscillating flow is characterized by five non-dimensional parameters: the two geometrical parameters L/D and A/D and the flow parameters, Reynolds number Re, the Stokes number α and the velocity ratio ϵ. The particle paths depend most strongly upon ϵ and the Strouhal number $St = D/\hat{W}T = 2\alpha^2/\pi\, Re$. Since the number of parameters involved in this problem is so large we have restricted the computations to one particular tube geometry, $A/D = 0.1$ and $L/D = 0.2$, which closely resembles the arterial prostheses in which we are interested.

Before considering more complicated waveforms we will discuss flows that oscillate sinusoidally. We firstly consider the case where $\epsilon = 1$, in which the boundary value of the stream function is given by (9). The flow is unidirectional and has zero value at the middle of the cycle. The structure of the flow cycle is presented by drawing the instantaneous streamlines at various times in the flow cycle. Figure 12 shows a sequence of calculated streamlines at $Re = 300$, $\alpha = 10$. The figures are produced by a computer contouring procedure by interpolation between the values of stream function at the mesh points. The coarseness of the mesh shows up in some regions where flow details are of the same size as the mesh length; the tube corrugation is 8 mesh lengths in the radial direction and 16 in the axial direction. The streamlines are not constrained to be parallel to the axis at their ends, and so in some cases appear to change direction abruptly at the entrance and exit. The streamlines on which the stream function has the wall value are marked by plus signs. As in steady flow their intersection with the wall is indeterminate to within half a mesh length and so this is not included. The values of stream function chosen for the streamlines shown are different on each diagram and so are not specified.

The maximum flow occurs at $t/T = 0$, which is the same as $t/T = 1$. At this phase in figure 12 there is a separation region of the same shape as that in steady flow at the same Reynolds number, but of larger size. As the volume flow rate decreases, the recirculating region grows in size, the separated region bulges to more than fill the corrugation and the flow becomes asymmetrical. The centre of the recirculating streamlines moves downstream up to $t/T = 0.35$ as it moves out of the corrugation. As the volume flow rate approaches zero at $t/T = 0.5$ this centre moves back and eventually, before disappearing at about midradius at t/T between 0.55 and 0.6, the recirculating streamlines cross the boundary into the upstream corrugation. The flow is at its most complicated in the low-velocity phase around $t/T = 0.5$. By $t/T = 0.65$ the flow becomes unidirectional and has the appearance of steady flow at low Reynolds number. It is noteworthy, however, that, as we saw in figure 6, the geometry in which we are studying oscillating flow is the one in which separation occurs at zero Reynolds number in steady flow. As the flow rate increases, the velocity remains unidirectional, except in the corrugation. The instantaneous streamlines with the wall value of the stream function are marked on the figures by plus signs. These represent separation streamlines when they spring from the wall and only when they are stationary or slowly changing. If α was small the flow would be quasi-steady throughout the cycle, but α is not small here. During the time interval from $t/T = 0.75$ through 1.0 to 0.1 there is a streamline leaving the wall close to the corner, the position of which is not changing throughout the whole of this interval. At $t/T = 0.75$ there is a closed loop of + points which is not attached to the wall, and this simply represents a circulatory flow; at this time the flow separates from the corner and almost immediately reattaches. From $t/T = 0.9$ onwards the separation streamline proceeds across the corrugation to reattach on the downstream wall. It remains

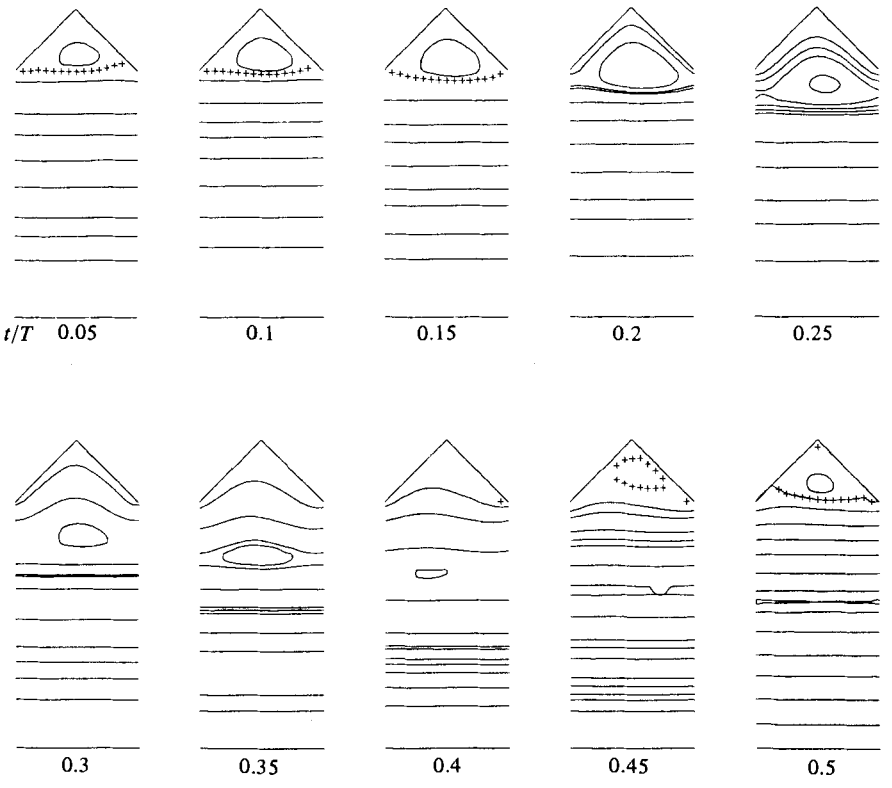

FIGURE 12. For caption see facing page.

approximately in the same position until separation ceases between $t/T = 0.15$ and 0.2. When the instantaneous streamlines with the wall value of stream function are rapidly changing as at $t/T = 0.5$ one cannot surmise that they represent a separation streamline.

It is remarkable that separation in unsteady flow takes place from the vicinity of the corner; whereas, in steady flow, separation first occurs at the apex as Reynolds number is increased. In unsteady flow, separation occurs whilst the flow near to the wall is accelerating.

We have already described the radial motion of the closed-loop streamlines. Simply by observation of the streamlines it is difficult to decide whether this vorticity is convected towards the axis or moves by diffusion away from its source at the wall. The paths of some particles labelled at $t = 0$ at positions within or near to a corrugation are shown in figure 13. The initial and final particle positions at $t/T = 0$ and 1.0 are given in the figure caption in terms of the coordinate system (i, j) shown in figure 1. Almost all particles within a corrugation leave the corrugation (are convected out) during the period and have a radial motion not very much less than their axial motion. Particles outside the corrugation move almost entirely in the axial direction and so convection plays no part in the radial motion of vorticity in this region. The Strouhal number based on the mean or amplitude of the velocity at a particular radius is small at positions nearer to the axis than the corners of the corrugations. At these positions the particles are convected axially many diameters in one period. During the interval in which the closed streamlines are at a particular

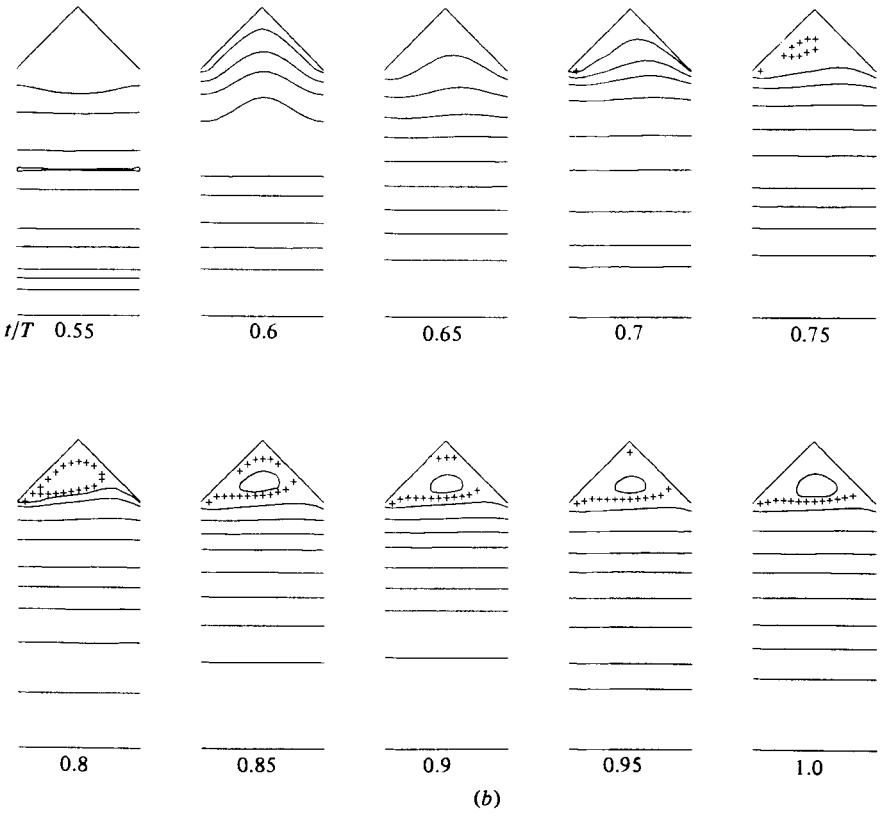

FIGURE 12. Instantaneous streamlines of oscillating flow; $\epsilon = 1$, $Re = 300$, $\alpha = 10$, $St = 0.2122$.

radial position outside the corrugations the axial convection is small because the closed loops instantaneously encompass a region of zero axial velocity. The particle paths in figure 13(*e*) are positioned near to the centres of the closed-loop streamlines at the times shown. The closed loops leave the corrugations by the mixed action of diffusion and convection. Their radial motion once outside the corrugations is almost entirely due to diffusion of vorticity. The migration downstream and upstream is the result of the nonlinearity of the problem and is caused by convection.

Turning now to figure 14 we see the effect of increasing α at the same value of Re. Because Re is the same in figures 12 and 14 the details of the flows in the corrugations is very little different over most of the cycle being dominated by separation of the flow, which is dependent on Re. The differences in the corrugation flows, except near zero volume flow rate, may not be entirely real. The range of stream function within the corrugation when separation has occurred is very small and only minute changes in ψ are required to produce observable differences. The difference at $t/T = 0.8$ in figures 12 and 14, for example, is also seen between the frames at times $t/T = 0.4$ and 0.9 in figure 16 where the patterns are identical when the computation has fully converged to the final solution.

The value of α in figure 14 is twice the value of figure 12, and so diffusion of vorticity is half as great as is evident at times $t/T = 0.3$–0.5. When the flow rate is near to zero at and just after $t/T = 0.5$ the streamline patterns appear very different in the two figures. As in oscillating flow in a cylindrical tube multiple undulations in the profile of the axial velocity occur at high α.

We consider now the waveforms with $\epsilon = 0$, which correspond to a sinusoidal

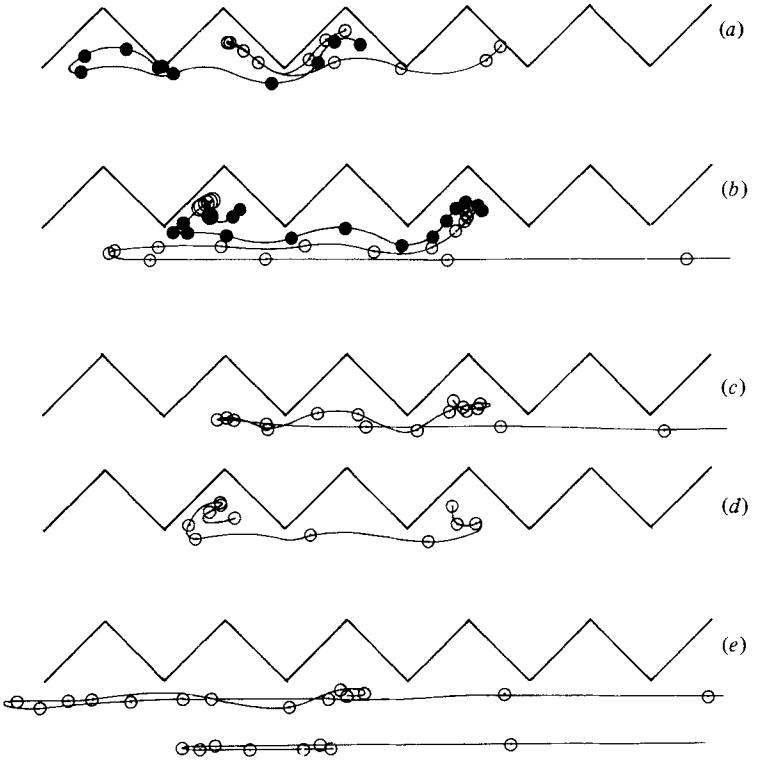

FIGURE 13. Particle paths of figure 12. Coordinates of the starting and end points at $t/T = 0$ and $t/T = 1.0$ are quoted in the system shown in figure 1: (*a*) 8, 37 to 28.6, 34.9 and 10, 35 to −16, 32.3; (*b*) 8, 34 to 202.6, 27.6 and 10, 34 to −21.9, 34.45; (*c*) 6, 34 to 135.4, 30.1; (*d*) 6, 35 to −22.8, 33.4; (*e*) 8, 30 at $t/T = 0.2$ to 137.5, 29.95 and 6, 23 at $t/T = 0.4$ to 291.4, 23.5.

oscillation of the volume flow rate about a zero mean value. A series of instantaneous streamlines is shown in figure 15 for $Re = 100$, $\alpha = 4.12$. When $\epsilon = 0$ the streamlines in consecutive half-cycles should be identical except for direction. Both halves are included to show that the computed differences are very small. The patterns are produced by running the programme until consecutive cycles are the same. This has to be a compromise between accuracy and computing time. When a comparison was made between figure 15 and the flow patterns produced with the same flow parameters but with $\epsilon = 1$ it was found that they were identical at corresponding times. In figure 16 the flow is shown at $\epsilon = 0$ for the same parameters as in figure 12. The identity obtained in the case of figure 15 leads us to expect correspondence at $t/T = 1.0$ ($= 0$) and at times in figure 16 which are less than 1.0 or more than 0 by half as much as in figure 12. In this case the correspondence is only found to be approximate, presumably because of nonlinear effects, which are more pronounced at higher Reynolds numbers. In figure 16 itself the flow patterns for $t/T = 0.05$–0.5 should be the mirror images of those for $t/T = 0.55$–1.0 if the computing has converged. This is seen to be the case except at $t/T = 0.4$ and 0.9 within the corrugation; here, where the velocity is low, only minute changes in ψ of the order of 1 part in 10^4 can produce the difference observed in the instantaneous streamline.

Particle paths for this zero-mean-flow case ($\epsilon = 0$) are shown in figure 17. As before, particles are convected out of the corrugation, but are convected radially by only very small amounts when they are away from the immediate neighbourhood of the corrugation. At all the positions shown radial convection produces an axial drift of the particle in one cycle, which in a cylindrical tube would be zero.

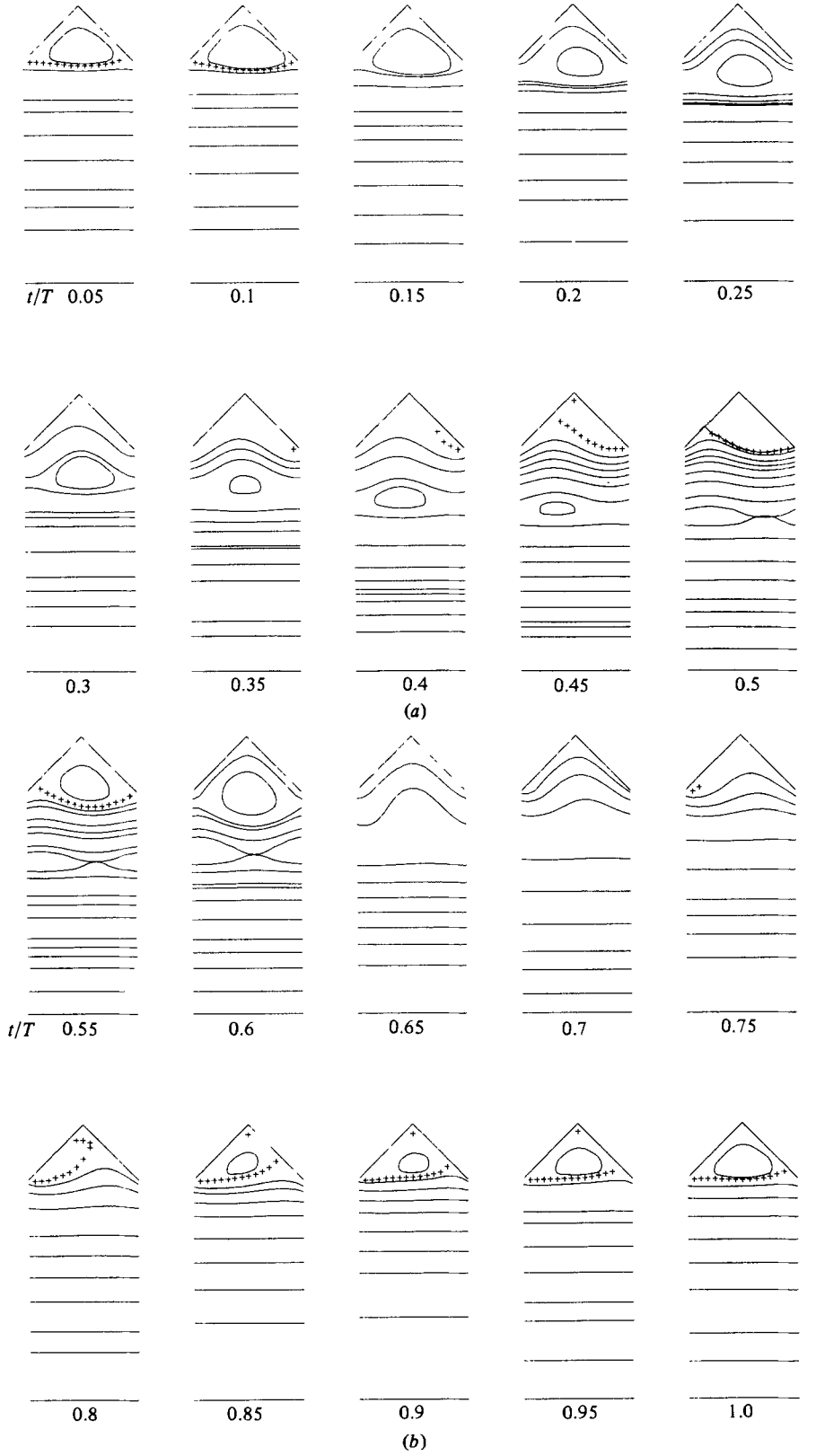

FIGURE 14. Instantaneous streamlines of oscillating flow; $\epsilon = 1$, $Re = 300$, $\alpha = 20$, $St = 0.8488$.

FIGURE 15. Instantaneous streamlines of oscillating flow; $\epsilon = 0$, $Re = 100$, $\alpha = 4.12$, $St = 0.1081$.

We are now in a position to discuss and summarize the relative effects of the flow parameters. It is found by comparing figure 16 with a computation at the same value of α but at $Re = 100$ rather than 300 that the rate of diffusion of the closed streamlines towards the axis is the same. This is as one would expect from the physical significance of α in a cylindrical tube (it is proportional to the ratio of the tube diameter to the distance that vorticity diffuses from the wall in one period of oscillation). The Reynolds number governs the stages in the cycle at which separation takes place and determines the convective transfer within the corrugations. The significance of the Strouhal number is apparent in the relative axial motions of particles at different radii.

The practical objective of the work is to determine whether a corrugated prosthesis is likely to produce clotting of blood because there are stagnant regions in the flow. We see from the particle paths already presented that it is exceedingly difficult to determine whether stagnant regions exist. A large amount of computation would be required to map out the regions of a corrugation in which the particles do not leave the corrugation. The character of the waveform will determine these regions. It is therefore only of direct bearing on the practical problem to look at the femoral-artery waveform in this same geometry. Before turning our attention to the practical case, brief reference will be made to the sinusoidally oscillating two-dimensional flows studied by Sobey (1980). The regions of interest diverge more than in steady flow because of the different applications. Sobey concentrates on zero and small mean flow. He discusses separation in terms of steady-flow concepts, whereas we prefer to view separation as evidenced by particles moving away from the wall. Where there is zero mean flow the main findings are similar in the two geometries, except where the effect

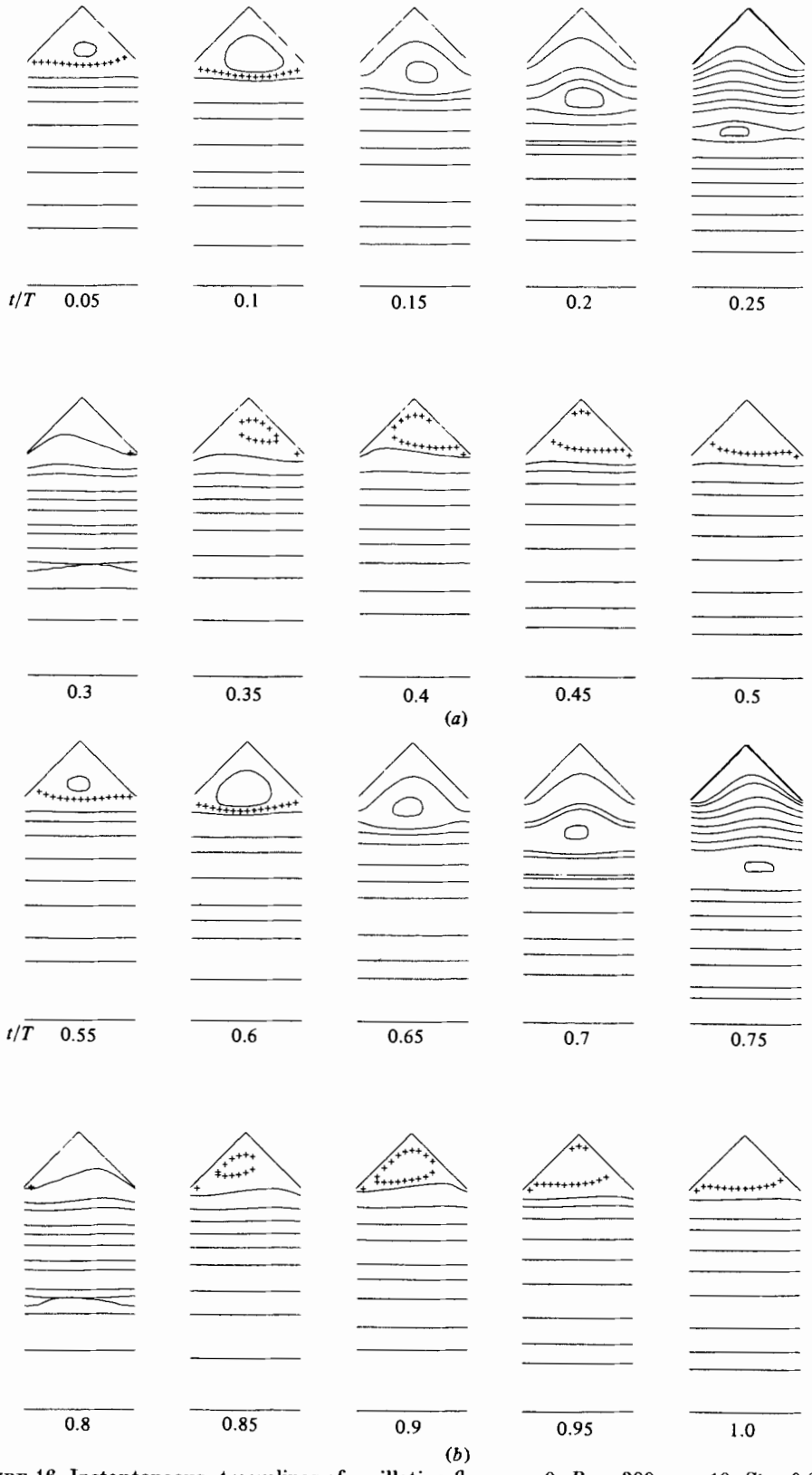

FIGURE 16. Instantaneous streamlines of oscillating flow; $\epsilon = 0$, $Re = 300$, $\alpha = 10$, $St = 0.2122$.

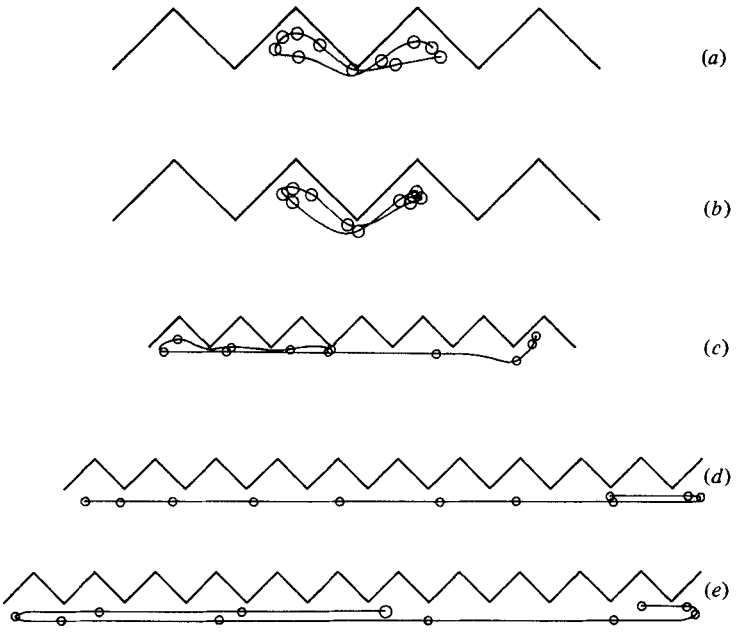

FIGURE 17. Particle paths of figure 15. Coordinates as in figure 12: (*a*) 10, 35 to 11, 33.8; (*b*) 8, 36 to 7.45, 35.1; (*c*) 6, 35 to −48.1, 31.8; (*d*) 0, 30 to −24.7, 28.6; (*e*) 8, 31 to −59.5, 29.6.

of the narrow central channel dominates in Sobey's case. When there is a mean flow the details of the two flows are different. The principal difference between the two cases is that with a narrow central channel mixing takes place over the whole cross section; in our case with corrugations which are relatively small mixing takes place within and bordering the corrugations.

Oscillating flow with mean flow equal to amplitude ($\epsilon = 1$) has been computed for a single widening in an otherwise cylindrical tube by Mirolyubov (1979). The shape of the wall is approximately sinusoidal, the α and Re are within our range, but A/D calculated from the maximum and minimum radii is 0.34. In this deep hollow, multiple circulating regions are found and multiple separation and reattachment is present throughout the cycle. The vortices do not appear to leave the corrugation as they did in Sobey's case. This work is similar to but not comparable with the cases presented here.

6. The equivalent cylindrical tube in oscillating flow

As we did for steady flow we may consider the equivalent cylindrical tube which has the same volume flow rate as in the corrugated tube for the same pressure gradient. For the oscillating component the treatment is a little more complicated and approximations have to be made in order to obtain a relationship which is easily applied. The steady component of the flow is considered in exactly the same way as for steady flow in §4. For the current geometry $A/D = 0.1$, $L/D = 0.2$ the mean pressure difference and the mean-flow results are shown in table 1 for steady flow and for the mean component of the unidirectional oscillating flow ($\epsilon = 1$). The cylindrical tube value of $Re\,p^*$ is 32. The equivalent cylindrical-tube diameters obtained from (23) are also shown. In this oscillating flow the Reynolds number of the mean flow is equal to that based on the amplitude. It appears from these results that for the

Re		100	200	250	300	500	700
Steady flow	p^*	0.56	0.28	0.23	0.192	0.12	0.085
($\alpha = 0$)	$Re\,p^*$	56	56	57.5	57.6	60	63.75
Oscillating flow	$\bar{p}^*$	0.645	0.31	0.2555	0.21	0.13	
($\epsilon = 1, \alpha = 4.12$)	$Re\,\bar{p}^*$	64.5	62	63.75	63	65	

Steady flow; mean $Re\,p^* = 58.5$ giving $D_e/D = 0.860$.

Oscillating flow; mean $Re\,\bar{p}^* = 63.65$ giving $D_e/D = 0.842$.

TABLE 1. Mean-flow components of the non-dimensional pressure drop in the corrugated tube

mean component $Re\,p^*$ is a function of α and even less dependent on Reynolds number than it is at $\alpha = 0$. This is surprising since the flow in the corrugations appeared to depend more strongly on Reynolds number than on α, but one does not see the mean component when viewing the instantaneous streamlines of a flow with a large oscillating component.

For oscillating flow the volume flow rate values are given and the computed pressure values, which have been Fourier-analysed to give the mean and fundamental frequency components of the amplitude; higher harmonics were less than 2 % of the fundamental. As for steady flow we write for the amplitude of the fundamental-frequency non-dimensional pressure

$$\hat{p}^* = kD^5, \tag{25}$$

where $k = (16\rho/\pi^2)\,\Delta\hat{p}/(L\hat{Q}^2) =$ constant by hypothesis. $\Delta\hat{p}$ is the amplitude of the fundamental component of the pressure difference across the corrugation and $\hat{Q}$ is the amplitude of the oscillating volume flow rate. For the equivalent cylindrical tube (suffix e) having the same value of k, the steady flow equation $p_e^* = 32/Re_e$ is replaced by

$$\hat{p}_e^* = f(\alpha_e)/Re_e, \tag{26}$$

where $f(\alpha_e) = 4\alpha_e^2/|1 - F_{10}|_e$. Here α_e is the equivalent cylindrical-tube value, which is $0.5D_e(2\pi/\nu T)^{\frac{1}{2}}$, and $|1 - F_{10}|_e$ is a function of α_e. $|1 - F_{10}|$, a complicated function of α, is tabulated by McDonald (1974), where it is called M'_{10}. As for steady flow, $Re_e = D\,Re/D_e$, Q being constant. We thus obtain

$$Re\,\hat{p}^* = \frac{D^2 4\alpha^2}{D_e^2|1 - F_{10}|_e}. \tag{27}$$

In order to simplify the computation of D_e it is necessary to approximate $|1 - F_{10}|_e$. Between $\alpha = 3.5$ and $\alpha = 20$, $|1 - F_{10}|$ is represented to better than 4 % by $0.547\alpha^{0.186}$, and so

$$\hat{p}^* = 7.31\alpha^{1.814}\,Re^{-1}\left(\frac{D}{D_e}\right)^{2.186}. \tag{28}$$

A more accurate representation in the restricted range $4 < \alpha < 8$ which gives $|1 - F_{10}|$ to better than 1 % is $0.503\alpha^{0.25}$. This gives

$$\hat{p}^* = 7.95\alpha^{1.75}\,Re^{-1}\left(\frac{D}{D_e}\right)^{2.25}. \tag{29}$$

D_e/D as calculated from (28) and (29) is plotted in figure 18 from data computed at $Re = 300$ and 100 which is presented in table 2. The dashed curve represents the more accurate values and their extrapolation. The curves are extended to $\alpha = 0$ to pass through 0.85 determined from steady-flow considerations.

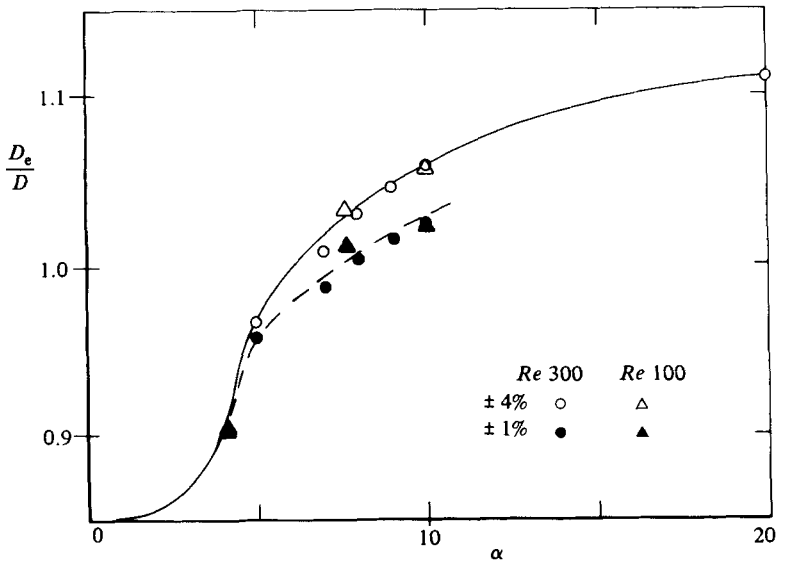

FIGURE 18. The diameter of the equivalent cylindrical tube in oscillating flow.

			$Re = 300$				
α	0	5	7	8	9	10	20
Cylinder $Re\hat{p}^*$	32	132.45	239.5	305.3	377.4	460.6	1717
Corrugated tube $Re\hat{p}^*$	57.6	146.7	246.3	293.8	359.1	422.0	1343
				(298.8)		(420.2)	
			$Re = 100$				
α		4.12		7.62		10.0	
Corrugated tube $Re\hat{p}^*$		119.2		274		423.8	
		(119.2)					

TABLE 2. The fundamental-frequency component of the non-dimensional pressure difference between the ends of the corrugation; values for $\epsilon = 1$ with $\epsilon = 0$ values are in brackets

This cumbersome analysis has been made in order to obtain the equivalent diameter which is of use medically when a corrugated prosthesis is being chosen to replace a diseased artery. A direct and simple relation between $Re\,p^*$ and α which fits the data of table 2 is presented as (31) in §7.2. We see no dependence of D_e or $Re\,p^*$ on Reynolds number, but have only investigated the two values $Re = 100$ and 300. Equations (29) and (33) give $D_e/D = 0.87\alpha^{0.067}$.

The values in table 2 show that whether $\epsilon = 0$ or 1 makes little difference to the resulting pressure drop; the maximum difference in $\hat{p}^*$ found in the few cases where comparison was possible is only 1.7 %.

7. Application to arterial prostheses

Arteriosclerosis is responsible for a large proportion of the deaths in America and Northern Europe, and haemodynamic factors are believed to play a role in the formation of atheroma at certain sites within the arterial tree (Middleman 1972). Atheroma is encountered most frequently where flow separation can occur, as

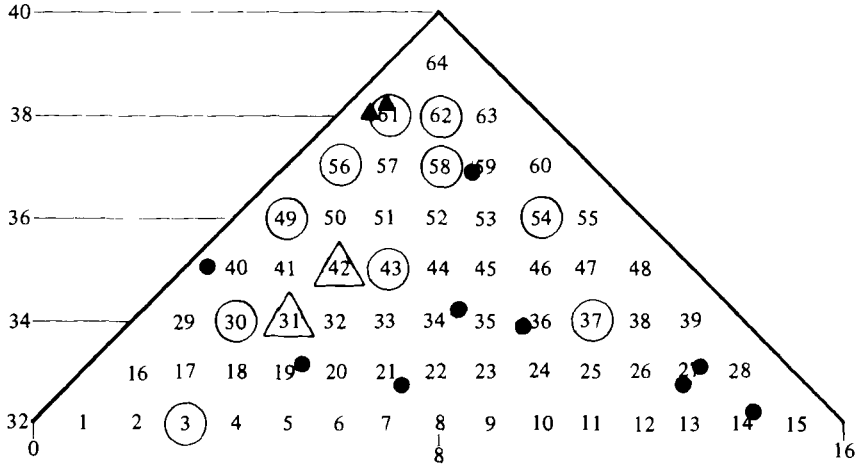

FIGURE 19. Particle positions in flow oscillating with a femoral artery waveform.

Initial position	Position after one period	
△	▲	Particle remaining in corrugation
○	●	Particle leaving and returning

evidenced by the work of Fry (1968) and Caro, Fitzgerald & Schroter (1971). When arterioscleriosis causes complete occlusion of an artery in the leg (iliac, femorals and popliteal), patients suffer pain on exercise and gangrene may develop. In these circumstances the only effective treatment is to bypass the obstructed artery. For the replacement of smaller arteries, of less than 6 mm diameter, such as the superficial femoral, tibial and coronary arteries, one of the patient's own veins is used as a bypass. LaSalle *et al.* (1982) have shown that in general vein grafts remain patent for much longer periods than prostheses of similar dimensions. When no vein is available a prosthetic artery must be used, and many of these have corrugated walls, so that they remain open when bent.

Blood tends to clot when in contact with a foreign material such as a prosthesis. Clotting is more likely in regions of stasis or regions of flow not washed out at each cycle of the heart beat. In arterial prostheses of small diameter the corrugations are relatively large and if the effect of the corrugations is to cause local stasis this may promote thrombus formation.

Whenever a main artery, for example the superficial femoral, is obstructed, a collateral pathway develops from small capillaries. It is essential that the impedance of any prosthesis used as a bypass is less than that of the collateral pathway: hence it is necessary to know how corrugations affect the resistance of artificial arteries. Additionally the resistance of the prosthesis is difficult to match to the adjoining vessels when the diameter is small, and as with a stenosis the presence of the collateral circulation may result in a slower flow if the resistance is too high.

In view of these facts it has seemed reasonable to consider the fluid mechanics of a corrugated tube with this application in mind. The aim was to investigate the possible occurrence of stagnant regions in the corrugations and to determine the pressure drop required to produce a given volume flow rate. The flow waveform was that of a normal human superficial femoral artery.

1	−25.02, 36.17	33	44.26, 27.56
2	−38.51, 34.85	34	109.23, 34.56
3	5.29, 33.17	35	72.43, 30.16
4	98.2, 31.2	36	40.3, 38.5
5	110.5, 30.8	37	15.02, 31.99
6	210.3, 31.95	38	4.87, 31.33
7	281.23, 37.08	39	−41.57, 35.3
8	286.31, 30.51	40	−26.5, 30.2
9	421.45, 32.58	41	−66.6, 26.8
10	457.73, 31.16	42	6.86, 38.14
11	548.19, 34.19	43	8.62, 36.88
12	485.64, 32.99	44	58.9, 36.47
13	460.79, 32.65	45	75.43, 36.32
14	248.46, 33.21	46	27.42, 33.54
15	79.36, 30.5	47	−8.34, 33.65
16	−65.45, 29.41	48	−101.00, 29.34
17	−69.74, 30.93	49	9.64, 33.87
18	−59.61, 32.50	50	−57.15, 35.4
19	21.1, 33.1	51	55.45, 34.30
20	108.2, 35.2	52	−83.58, 31.4
21	135.6, 33.75	53	−12.79, 32.84
22	143.8, 30.7	54	3.39, 35.05
23	141.94, 34.9	55	25.08, 38.42
24	136.58, 37.4	56	14.17, 32.22
25	290.8, 32.2	57	−1.97, 30.83
26	296.9, 34.56	58	8.35, 34.24
27	89.33, 36.42	59	47.91, 30.83
28	−23.76, 30.6	60	−12.38, 35.22
29	−25.5, 36.17	61	13.1, 33.06
30	7.28, 32.76	62	12.8, 32.73
31	6.56, 38.03	63	−86.32, 35.32
32	−89.67, 29.32		

TABLE 3. Coordinates of the particles initially at the positions shown in figure 19 after one period of oscillation of the femoral artery waveform. Coordinate system of figure 1.

7.1. *Computation of the particle paths*

In the numerical analysis it was necessary only to replace the sinusoidally oscillating volume flow rate Q by a superfical femoral artery waveform. The flow waveform was taken from the determination in a normal human artery by Dedichen & Kordt (1974). This was Fourier-analysed to determine the mean and the first six harmonics, and these are quoted in table 4. The period of the wave was 1.0 s, the mean Q was 1.6 ml/s, the maximum Q was 12.3 ml/s, and the minimum Q was −2.6 ml/s. The geometry of the corrugated tube was as before, $L/D = 0.2$, $A/D = 0.1$. To obtain the Reynolds numbers it was assumed that the diameter D was 5 mm and the kinematic viscosity 4 mm^2/s. The flow was expressed in terms of the value of the stream function at the wall and the value of this at each time step was determined from a Fourier synthesis. The instantaneous streamlines computed were as would be expected from the results already presented. Particle paths were determined for fluid particles initially at each of the 64 mesh intersections in one corrugation. The initial positions of the particles are numbered from 1 to 64 in figure 19. The particle positions after one period are listed in table 3. The particles which at the end of the period remained in the corrugation which they initially occupied are marked in the figure. Two particles remain in the corrugation throughout the period. The other 10 marked particles leave

the corrugation during the cycle and return to the positions indicated. All but one of these particles go into the adjoining corrugation, particle 30 goes into the next corrugation but one before returning. One notices that these particles will leave the corrugation in the next cycle or the next cycle after that.

The particles were placed at the mesh intersections. It is evident that the mesh is coarse and that particles at adjacent mesh points are convected to widely different final positions. Since the computing time required for a smaller mesh would be prohibitively long, the results as presented are the best that we can achieve, but have the possibility of error in the fine scale. The results suggest that the mixing of fluid near to the wall is more energetic than in the case of a cylindrical tube and that there is no indication of any stagnant regions forming on a timescale of the size of a period of the oscillation. It appears that corrugated prostheses will not fail because of stagnant pockets of fluid in the corrugations.

The particle number 64 has been omitted from table 3. The numerical analysis is such that this particle does not migrate. This region was investigated by truncating the corrugation at ordinate 39 and inserting particles at coordinates 7.5, 38.5 and 8.5, 38.5. These particles were washed away and the rest of the particles executed essentially the same paths as before.

7.2. *The non-dimensional pressure difference between the ends of the corrugation*

As with sinusoidally oscillating flow, the non-dimensional pressure gradient $\hat{p}^*$ was determined for the femoral-artery waveform. The resulting values were Fourier-analysed to give the components shown in table 4. The non-dimensional pressures shown are based on the different peak velocities of each harmonic component. The Reynolds numbers are based on the same velocities and the diameter D. The values of $\hat{p}^*$ were also computed on the assumption that the Fourier components were present alone, that is, without the nonlinear interactions which are present. This computation may be made using (29). Alternatively, without recourse to the equivalent diameter, we may directly analyse the values of table 2 to give

$$Re\,\hat{p}^* = 58 + 3.56\alpha^{2.02} \quad (4 \leqslant \alpha \leqslant 20). \tag{30}$$

This equation is accurate to within 2.5 %. With very little extra inaccuracy we may also write

$$Re\,\hat{p}^* = 10.86\alpha^{1.6}. \tag{31}$$

From the results in table 4 we see that the pressure gradient that produces the given flux in the composite femoral wave is within about 10 %, in all cases, of the value obtained when the components are present alone. In the case of a sinusoidal oscillation the values of $Re\,\hat{p}^*$ for the corrugated tube lie above those of the equivalent cylindrical tube when $\alpha < 7.6$; above this α the cylindrical tube values are the greater. It happens, presumably fortuitously, that the $Re\,\hat{p}^*$ values for the components of the femoral waveform lie almost exactly on the cylindrical-tube curve, with the exception of the fundamental component, which lies midway between the cylindrical- and corrugated-tube curves. The nonlinear effects of the corrugation and of the composite waveform happen to be equal and opposite. The value of the product of the mean values $\overline{Re}\;\overline{p^*}$ was found to be 58.0, which is close to the steady-flow value quoted in table 1. The corresponding equivalent diameter divided by the maximum diameter calculated from (23) is thus 0.861.

Frequency (Hz)	α	Q amplitude (ml/s)	Re	$\hat{p}^*$	$\hat{p}^*$ from (31) for harmonic components present separately
1	3.76	3.04	161.7	0.600	0.68
2	5.31	3.24	171.7	0.871	0.94
3	6.51	2.57	136.2	1.506	1.575
4	7.52	1.14	60.6	4.380	4.42
5	8.40	0.60	31.8	10.44	10.06
6	9.21	0.39	20.75	19.17	18.01

TABLE 4. The non-dimensional pressure difference across the corrugation. Superficial femoral artery waveform. Mean volume flow rate = 1.57 ml/s, mean Reynolds number = 100.

7.3. *Conclusions*

The results of this work on the application to corrugated prosthetic arteries are negative. There appears to be no fluid-mechanical reason why corrugated tubes should perform worse than prostheses with a uniform diameter or even the patient's own veins. Figliola & Mueller (1981) show that regions of slowly moving separated flow correlate with clinical findings of thrombus formation, and also that separations that wash out at each cycle seem not to produce these adverse effects. Compared with cylindrical tubes there is increased mixing in the wall region of corrugated tubes. There is no indication of the formation of stagnant regions in the corrugations when a normal arterial waveform is considered. It is, however, well known that the waveforms in atherosclerotic arteries are far from normal, even after a bypass graft operation.

The non-dimensional pressure differences found from the femoral-artery waveform analysis are less than 10% different from the values calculated when the harmonic components are present alone. The decrease of resistance with frequency α is shown by the 25% increase in D_e/D up to $\alpha = 20$ in figure 18. The resistance of the cylindrical tube increases by a large factor as α increases, owing principally to inertia effects. McDonald (1974) shows in his figure 6.5 that the flux for a given pressure gradient drops by a factor of ten between $\alpha = 0$ and $\alpha = 10$. Frictional effects produce wave attenuation, but the magnitude of this in a short length of normal artery is very small. It is unlikely that the small differences in frictional effects that we have determined will have a noticeable effect on the flux.

It must be stated that mismatching of the diameter will produce much larger effects on the resistance of the tube. The pressure gradient for a given flux depends on a high power of the diameter; the fourth power in steady flow (23) and the 2.25 power in oscillating flow (29).

8. General conclusions

The flow in a corrugated tube has been investigated for steady and oscillating flows of different waveforms. In all cases instantaneous streamlines and particle paths have been calculated and a study made of the effect of the variation of the parameters of the problem.

In steady flow the geometry (L/D and A/D) was varied as well as the Reynolds number. The most striking feature of the flow is the onset and growth of separation. There is no separation when L/D is large and A/D and Reynolds number are small. As these parameters are changed to produce separation, this always occurs first at

the apex of the corrugation. The parameters interact so that, for example, the critical L/D for separation increases as either Re or A/D increase. Separation was found to occur at zero Reynolds number for small-enough L/D and large-enough A/D.

In unsteady flow the non-dimensional frequency α or St enters as well as the ratio ϵ of the mean of the flux to its amplitude. Calculation of these flows was restricted to one pair of values of A/D and L/D. The flux ratio ϵ was found to have only a small effect, except on the timescale and thus on the diffusion of vorticity from the wall. Regions of quasi-steady separation at maximum flux were found. The separation was in these cases at or near to the corner rather than at the apex of the corrugation. The results showed enhanced mixing due to convection in the radial direction within and adjacent to the corrugations. It was found that the flow patterns were characterized in the corrugation by the Reynolds number and in the central flow by the Stokes number α.

The occurrence of persistent stagnation regions in the corrugation was investigated for an arterial waveform, and it was concluded that such regions do not exist in the geometry considered and the waveform studied. If there remains a fluid-mechanical reason why the failure rate of corrugated prostheses is higher than that of cylindrical tubes it may be that the waveform of the oscillations departs from the normal. In the cases that we have considered the mixing in the wall region was enhanced by the presence of the corrugations.

The resistance of the tubes was related to that of a cylindrical tube. One would expect increased mixing to increase the resistance. In steady flow the resistance is a function only of the product of Reynolds number and non-dimensional pressure difference which in turn depends mainly on A/D. The resistance increases as A/D increases, as one would expect. Resistance also increases with increasing Reynolds number and with decreasing L/D. In the range we have studied the latter effect is small. Some computations made to compare with the results of Deiber & Schowalter (1979) have shown large effects when L/D is greater than 1. Comparison with these results obtained for a sinusoidally varying tube radius shows that the difference in geometry produces very small changes in the non-dimensional pressure drop at the same L/D and A/D. The A in A/D is equated to twice the amplitude of the variation of the tube radius. This equivalence may well not hold for small values of L/D. In oscillating flow the resistance compared with that of a cylindrical tube decreases as α increases; the change is about 30% from $\alpha = 0$ to $\alpha = 20$. The resistance of a cylindrical tube has a very much stronger increase with frequency due to inertia effects. The changes in resistance due to the corrugations are small compared with the total resistance to the flow.

We had hoped that a fuller investigation of unsteady separation would have been possible. In general one can see that the instantaneous streamlines and the particle paths give the same impression of the flow. When there is an instantaneous streamline springing from the wall having a stream-function value equal to the wall value, this would be a separation streamline in steady flow. To investigate the unsteady separation it would be necessary to follow the paths of a large number of particles and employ a fine mesh in this region. This is not possible in the present work, where a large field has to be covered at the same time as investigating the fine detail.

We are pleased to take this opportunity to acknowledge the encouragement and assistance given by D. Charlesworth of the University of Manchester Department of Surgery. C. N. Savvides also gratefully acknowledges the University of Manchester Post Graduate Scholarship which he has received for two years.

The final form of the paper owes much to the helpful suggestions of the referees, whose careful scrutiny we are pleased to acknowledge.

REFERENCES

AZZAM, M. I. S. & DULLIEN, F. A. L. 1977 Flow in tubes with periodic step changes in diameter: a numerical solution. *Chem. Engng Sci.* **32**, 1445.

BATRA, V. K., FULFORD, G. D. & DULLIEN, F. A. L. 1970 Laminar flow through periodically convergent–divergent tubes and channels. *Can. J. Chem. Engng* **18**, 622.

BUTLER, G. A. 1979 Blood flow in arteries with and without prosthetic inserts. Ph.D. thesis. University of Manchester.

CARO, C. G., FITZGERALD, J. F., & SCHROTER, R. C. 1971 Atheroma and arterial shear. *Proc. R. Soc. Lond.* B **177**, 109.

DEIBER, J. A. & SCHOWALTER, W. R. 1979 Flow through tubes with sinusoidal axial variations in diameter. *AIChE J.* **25**, 638.

FIGLIOLA, R. S. & MUELLER, T. J. 1981 On the hemolytic and thrombogenic potential of occluder prosthetic heart valves from in vitro measurements. *Trans. ASME* K: *J. Biomech. Engng* **103**, 83.

FRY, D. L. 1968 Acute vascular endothelial changes associated with increased blood velocity gradients. *Circulation Res.* **22**, 165.

GERRARD, J. H. 1971 The stability of unsteady axisymmetric incompressible pipe flow close to a piston. *J. Fluid Mech.* **50**, 625.

GILLANI, N. V. & SWANSON, W. M. 1976 Time dependent laminar incompressible flow through a spherical cavity. *J. Fluid Mech.* **78**, 99.

LASALLE, A. J., BREWSTER, D. C., CORSON, J. D. & DARLING, R. C. 1982 Femoropopliteal composite bypass grafts; current status. *Surgery* **92**, 36.

MACAGNO, E. O. & HUNG, T. K. 1967 Computational and experimental study of a captive annular eddy. *J. Fluid Mech.* **28**, 43.

MCDONALD, D. A. 1974 *Blood Flow in Arteries.* Arnold.

MIDDLEMAN, S. 1972 *Transport Phenomena in the Cardivascular System.* Wiley.

MIROLYUBOV, S. G. 1979 Pulsating flow of a Newtonian liquid through an axisymmetric tube with local enlargement. *Izv. Akad. Nauk SSSR, Mekh. Zhid. i Gaza* no. 6, 125.

MOFFATT, H. K. 1964 Viscous and resistive eddies near a sharp corner. *J. Fluid Mech.* **18**, 1.

PEARSON, C. E. 1965 A computational method for viscous flow problems. *J. Fluid Mech.* **21**, 611.

ROACHE, P. J. 1972 *Computational Fluid Dynamics.* Hermosa.

SMITH, F. T. 1976 Flow through constricted or dilated pipes and channels: Parts I and II. *Q. J. Mech. Appl. Maths* **29**, 343 and 365.

SOBEY, I. J. 1980 On flow through furrowed channels. Part 1. Calculated flow patterns. *J. Fluid Mech.* **96**, 1.

THOMAN, D. C. & SZEWCZYK, A. A. 1964 Time dependent viscous flow over a circular cylinder. *Phys. Fluids* **12**, II–76.

WILLIAMS, G. P. 1969 Numerical integration of the three-dimensional Navier–Stokes equations for incompressible flow. *J. Fluid Mech.* **37**, 727.